

Enhancement of Superconductivity upon reduction of carrier density in proximitized graphene

Gopi Nath Daptary,¹ Udit Khanna,¹ Eyal Walach,¹ Arnab Roy,¹ Efrat Shimshoni,¹ and Aviad Frydman¹

¹*Department of Physics, Jack and Pearl Resnick Institute and the Institute of Nanotechnology and Advanced Materials, Bar-Ilan University, Ramat-Gan 52900, Israel*

(Dated: March 10, 2022)

The superconducting transition temperature (T_c) of a single layer graphene coupled to an Indium oxide (InO) film, a low carrier-density superconductor, is found to increase with *decreasing* carrier density and is largest close to the average charge neutrality point in graphene. Such an effect is very surprising in conventional BCS superconductors. We study this phenomenon both experimentally and theoretically. Our analysis suggests that the InO film induces random electron and hole-doped puddles in the graphene. The Josephson effect across these regions of opposite polarity enhances the Josephson coupling between the superconducting clusters in InO, along with the overall T_c of the bilayer heterostructure. This enhancement is most effective when the chemical potential of the system is tuned between the charge neutrality points of the electron and hole-doped regions.

Low carrier-density superconductivity has been a topic of great interest in condensed matter research since its discovery in SrTiO₃ [1]. In conventional BCS superconductors, the critical temperature, T_c , is known to increase with increasing carrier density (n) [2]. Contrarily, experiments on a number of exotic low density superconductors, such as Li-intercalated layered nitrides [3, 4], underdoped La_{2-x}Sr_xCuO₄ [5] etc., detected an enhancement of T_c with decreasing n . These results were interpreted as evidence for a non-BCS mechanism of electronic pairing, such as electron-electron (rather than electron-phonon) interactions [6, 7]. To date there is no known mechanism for enhancement of T_c upon reducing n for a BCS superconductor. In this paper, we present results of a conventional superconducting system in which T_c is largest close to a charge neutrality point (CNP) for which n can be extremely small.

Two-dimensional superconductors, in which the chemical potential can be modulated by gate voltage (V_g) are an ideal system for approaching the ultra low carrier-density regime. Graphene [8] is unique in this sense since the low energy dispersion is linear with momentum, i.e., the conduction and valence band touch at discrete points (Dirac points) resulting in a gapless semiconductor [9]. Hence n can be tuned through the CNP and may, in principle, be as small as desired. In this paper we show that coupling graphene to a highly disordered, low-density superconductor gives rise to unique situation as the superconducting islands induce hole-doped regions within graphene, thus generating two CNPs (discussed later) in place of the global Dirac point for the non-proximitized graphene. This leads to a unique situation where superconductivity is enhanced with decreasing n and is strongest close to the average CNP. We present a model to explain this extraordinary result based on the Josephson effect between regions of opposite polarity within the graphene. We show that the Josephson coupling between different superconducting regions is maximal when the system is tuned approximately half-way

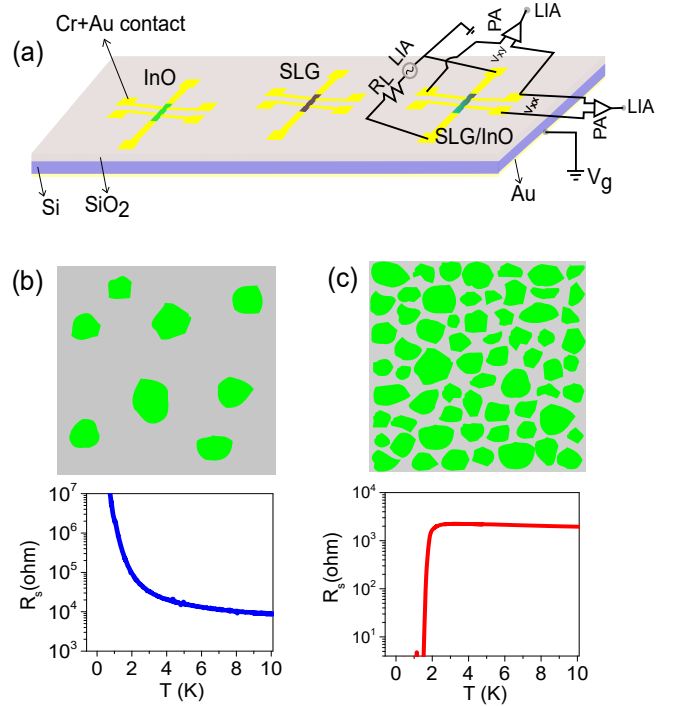


FIG. 1. (a) A schematic diagram of the devices (From left: InO, SLG and an InO/SLG heterostructure). The longitudinal and transverse voltages are measured by a lock-in amplifier (SR 830) after amplification of the signals by a low noise preamplifier (PA-SR552). The carrier density is modulated by the back gate voltage V_g applied to the contact at the bottom of the Si. (b) and (c) Sketches of the superconducting islands and the resistance versus temperature curves of samples I and S respectively.

between the charge neutrality points of the electron and hole-doped regions. This occurs close to the global CNP of the graphene layer in the heterostructure.

The experiments were performed on heterostructures of single layer graphene (SLG) and thin amorphous indium oxide (InO). We use CVD grown SLG sheets transferred onto 285 nm SiO₂ on top of a Si wafer as a 2D

material. The sample was patterned into a Hall bar geometry by standard e-beam lithography and contacted to Cr/Au leads (5 nm/30 nm). It was then covered by a 30 nm thick InO film via a second lithography step. For reference, we prepared similar geometries of bare graphene and bare InO [see Fig. 1(a)]. The channel length and width of the sample are 150 μm and 50 μm respectively. The carrier density of the graphene device was modulated by changing the gate voltage applied to the back side of Si wafer. The device structure along with the electrical connections are shown in Fig. 1(a). Measurements were performed in a wet He-3 system at temperatures down to 0.3 K.

InO is a low density superconductor where n can be controlled between $\sim 10^{19} - 10^{20} \text{ cm}^{-3}$ by changing the O_2 partial pressure during film deposition [10]. For large n , the critical temperature, T_C can reach $\sim 3.5\text{K}$ and the coherence length ξ is 30 – 50nm [11, 12]. Decreasing n causes the InO film to undergo a transition from a superconducting state to an insulating state. Nevertheless it has been shown that in both phases, the film includes emergent superconducting puddles, with sizes of a few μm , embedded in an insulating matrix [13–15]. Indeed, comparable finite energy gap, Δ , and vortex motion were measured in both phases [12, 16–20]. The difference between a superconducting film and an insulating one lies in the global superfluid density which depends on the Josephson coupling between superconducting puddles [21]. This is illustrated schematically in Fig. 1 panels b and c which show the resistance versus temperature curves of two InO films: one insulating, denoted as sample I [panel (b)] and one superconducting denoted as sample S [panel (c)] together with sketches of the inherent superconducting granularity. In the insulating phase the superconducting islands are sparse and decoupled, so that superconductivity is present only locally, while in the superconducting phase Josephson coupling percolates across the sample and global superconductivity is achieved.

In this paper we discuss the results from two of the samples, Gr/S and Gr/I, which are heterostructures of SLG and a thin InO layer in the superconducting or insulating phase respectively. A second superconducting sample (Gr/S2) showed similar results as shown in the supplementary material. In a previous work we presented results on sample Gr/I [22]. In such a system the rather sparse InO superconducting puddles proximitize the underlying regions in the graphene sheet, at the same time hole-doping them relative to the remaining SLG. Hence, the system includes a second charge neutrality point in addition to the usual CNP of the overall electron doped graphene (DP_e) [22]. This point, dubbed the “hole Dirac point” (DP_h), gives rise to an additional peak in the resistance versus gate voltage (R - V_g) curve as seen in Fig. 2(a). Unlike most experiments of SLG coupled to a BCS superconductor, the low carrier density of InO

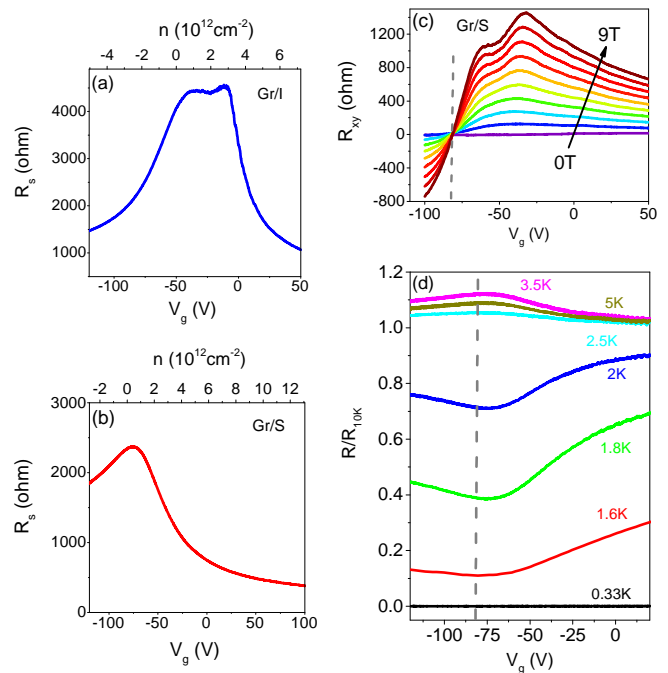


FIG. 2. (a) and (b) Sheet resistance, R_s , as a function of V_g of sample Gr/I and sample Gr/S respectively at zero magnetic field. The measurements were performed at $T = 1.7 \text{ K}$ for Gr/I and at $T = 5 \text{ K}$ ($T > T_C$) for Gr/S. (c) Hall resistance, R_{xy} , as a function of V_g at different magnetic fields ($B = 0 - 9\text{T}$ in steps of 1T) at $T = 1.7\text{K}$ of sample Gr/S. Note that the charge neutrality point is at a gate voltage of $V_d = -81.5\text{V}$. (d) Sheet resistance, normalized by the resistance at 10K, as a function of V_g at different T of sample Gr/S. The slight difference between the CNP extracted from the Hall measurement and that of the resistance peak is attributed to the disorder of the sample which leads to some spatial distribution of n . Note that the resistance reaches a maximum at $T = 3.5\text{K}$. This is due to the non-monotonic nature of indium oxide film transport [20].

(a few orders of magnitude smaller than conventional superconductors) makes it experimentally possible to access both CNPs, i.e DP_e and DP_h in sample Gr/I. Our results also indicate that in samples for which the InO film is closer to the superconducting transition, the separation (in energy) between DP_e and DP_h is larger [22], thus making it experimentally difficult to probe both CNPs. Nevertheless, a large region around the midpoint between DP_e and DP_h is accessible.

In the current work, we focus on Gr/S. Figure 2(b) shows that for high temperatures T significantly above T_C , one resistance peak is observed. Hall effect measurements [see Fig. 2(c)] identify this resistance peak as the charge neutrality point of the system. Surprisingly, as the temperature is lowered close and below T_C , the peak at the CNP turns into a dip which becomes sharper with decreasing T , until a sufficiently low temperature at which the sample becomes superconducting in the entire V_g regime [see Fig. 2(d)]. This dip implies that superconductivity is *strongest* close to the CNP.

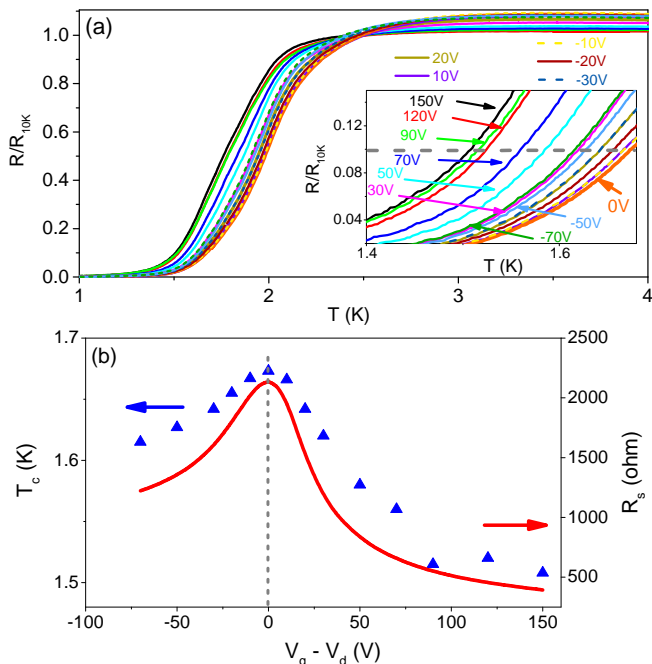


FIG. 3. (a) Sheet resistance, R_s , normalized by the resistance at 10K, as a function of temperature at different gate voltages relative to the CNP, $V_g - V_d$, of sample Gr/S. Inset: A zoom on the small temperature range highlighting the evaluation of T_c with gate voltage. (b) T_c and R_s at $T = 5$ K as a function of $V_g - V_d$ measured at $B = 0$ T.

This notion is further supported by the $R(T)$ curves at different V_g presented in Fig. 3 for sample Gr/S. For all gate voltages the heterostructure shows superconductivity at low temperatures. However, it is seen that T_C (defined as the temperature at which the resistance drops to 90% of the normal sheet resistance at 10K) systematically increases as n decreases and reaches a maximum around the high-temperature CNP. This is in stark contrast with the common behavior of conventional superconductors and with previous experiments of Sn dots on graphene [23] which exhibit a minimum of T_C at the CNP.

A possible explanation for such behavior would be to invoke a non-BCS pairing mechanism in the proximitized islands in graphene. Such mechanisms have been used to explain the enhancement of superconductivity of exotic low density superconductors [7]. However there seems to be no reason to assume that superconductivity in InO is of unconventional nature and hence any superconducting regions in the proximitized graphene are unlikely to show non-BCS properties. Instead we suggest that in our samples, the graphene provides a medium for Josephson coupling between the superconducting clusters of InO, thereby enhancing the superfluid stiffness. We emphasize that, just as in the bare InO thin films, T_C is dictated by the stiffness which controls phase fluctuations among the

superconducting clusters, and not by the pairing amplitude. In the Gr/S heterostructure, it is maximal close to the average CNP because (as shown below) Josephson effect through puddles of opposite polarity in the graphene layer is strongest when their average density is close to zero.

In clear contrast to sample Gr/I, in sample Gr/S the volume fraction of superconducting islands within the InO is roughly equal to that of the insulating regions (see Fig. 1c). In the underlying SLG, this generates large hole-doped puddles with proximity-induced superconductivity embedded in an electron-doped background. These superconducting islands are absent at temperatures far above T_C since no emergent granularity is expected in the normal state [15] of InO. In this case, both electron-doped and hole-doped regions in the SLG contribute equally to the transport. Thus, Hall measurements feature a CNP (consistent with the observation of a peak in the (longitudinal) resistance as a function of the gate voltage [Fig. 2(d)] for T larger than 2.5K) when the average density of the sample is zero, i.e. the electron and hole densities are roughly equal. However, as T is reduced and transport flows mostly through the superconducting islands, the finite resistance is dominated by patches of the SLG underlying the narrow constrictions between them. These effectively become SNS junctions where the S regions are hole-doped compared to the N region.

The proper model for the system at low T is therefore a random array of Josephson junctions, where the Josephson coupling (ultimately dictating T_C of the network) is provided by SNS constrictions of varying sizes. To analyse their V_g -dependence, we consider a single SNS weak link and calculate its critical current (I_c) at $T = 0$ (see Supplementary Material for details). The Fermi energy in the normal (N) region (E_F) is assumed to be positive, while the Fermi energy in the superconducting (S) regions ($E'_F = E_F - U$) is negative. The difference between the two (U) is assumed to arise from the difference in the electrostatic potential induced by the superconducting puddles in the InO. When V_g is varied, E_F and E'_F shift while maintaining U fixed. The Josephson coupling of the junction is proportional to its critical current I_c . The length (L) of the weak link is assumed to be much smaller than the superconducting coherence length (ξ). In this limit, the contribution to the supercurrent from the continuum states may be neglected, and only the contribution from the subgap ($\epsilon < \Delta$) Andreev bound states needs to be computed [24, 25]. We also assume $L \ll W$ (the width of the link) so that there is a single bound state for each transverse wave vector.

Graphene SNS junctions have been studied previously in great detail [26–29], including in the limit considered here [26]. However the previous works only considered the case where superconducting regions were heavily doped compared to the normal region. These studies find that I_c is minimal at the Dirac point of the normal re-

gion and increases monotonically as the carrier density n is increased. This behavior is compatible with, e.g., the experiments based on granular Sn islands deposited on a single layer of graphene [23], where the S regions are metallic superconductors.

Our model goes beyond previous works in that we relax the assumption of very heavily doped superconducting regions. Furthermore, in our case the unique scenario dictated by the experimental system forces us to explore the regime where the carrier densities in the superconductor and normal regions are close to each other in magnitude, but opposite in sign. We evaluate the spectrum of the subgap Andreev bound states ϵ_q^{ABS} in such a Josephson junction as a function of the phase difference between the superconducting regions (ϕ). The equilibrium Josephson current may be found through,

$$I(\phi) = -4 \frac{e}{\hbar} \sum_q \frac{\partial \epsilon_q^{\text{ABS}}}{\partial \phi}. \quad (1)$$

Here the factor of 4 accounts for the spin and valley degeneracies. The critical current I_c is simply the maximal value of $I(\phi)$. As explained earlier, the behavior of I_c as a function of the Fermi energy is expected to follow the variation of T_C as a function of V_g in the sample Gr/S.

Fig. 4 shows the variation of the critical current as a function of the Fermi energy (E_F) in the normal region. Note that in our convention, DP_e (DP_h) appears at $E_F = 0$ ($E'_F = E_F - U = 0$) which corresponds to the left (right) end of Fig. 4. The curve shown in Fig. 4 was obtained after averaging I_c over several values of L (length of the SNS junction). The averaging removes spurious oscillatory features which depend on the value of L (see SM), leaving behind a prominent gross feature: a broad maximum in the doping dependence of I_c . This captures the situation in the experimental system, where the percolating network of superconducting islands is expected to be dominated by several, most resistive, hotspots (or Josephson junctions) of varying lengths.

When the Fermi energy is close to the DP_e our results match those reported in Ref. [26], since the carrier density in the superconductors is quite large ($|E'_F| \gg E_F$). With increasing E_F , the average I_c increases monotonically until $E_F \sim U/2$. At this point, the carrier density in the S and N regions is equal, and the average carrier density of the SLG is expected to be close to zero. Hence, we expect $E_F = U/2$ to be close to the global CNP in our heterostructure (sample Gr/S). Increasing E_F beyond $U/2$ drives the system into a previously unexplored regime, where the carrier density of the normal region is larger than that of the superconductors. Andreev reflection at the two N-S interfaces is highly suppressed in this regime, leading to a rapid decrease in I_c despite the increase of carrier density in the normal region. For this reason, we observe the largest Josephson effect near $E_F = U/2$. Since the average CNP in sample Gr/S was

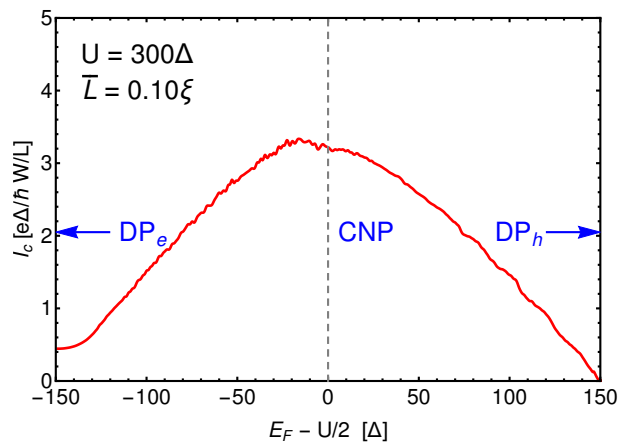


FIG. 4. The critical current (I_c) as a function of the Fermi energy relative to the CNP (in units of Δ). The leftmost (rightmost) energy corresponds to the DP_e (DP_h). At the CNP, the carrier densities in the electron and hole regions are equal, so that the average density is zero. Contrary to the standard picture, I_c is largest in the regime where the (net) carrier density is very small. This is a consequence of the opposite polarity of the superconducting and normal regions. The red curve shows I_c after averaging over the length (L) of the SNS junction (keeping $\bar{L} = 0.1\xi$), in order to remove the length-dependent features and account for the disordered nature of the superconducting puddles. Here, the value of the electrostatic shift is $U = 300\Delta$.

identified with this point, we expect to have the strongest Josephson coupling between the superconducting islands, and the largest enhancement in T_c , at the CNP. This is indeed consistent with our experimental observations (Fig. 3). Theoretically, I_c has two local minimas at the Dirac point of the normal region ($E_F = 0$) and that of the superconducting region ($E_F = U$). In our experiments however, we were unable to reach the two Dirac nodes, and only observed that the T_C keeps decreasing away from the CNP.

In summary, we have shown that coupling a SLG to a disordered, low-density superconductor leads to the unique result where superconductivity is strongest close to the average charge neutrality point of the graphene, in stark contrast to the situation in systems of SLG coupled to high-density superconductors. We ascribe this to the presence of regions of opposite charge polarity induced within the graphene which acts as a coupling medium for superconducting islands. This newly explored regime provides access to Andreev reflections in low-density S-N junctions, where the carrier density in the superconducting regions is possibly lower than the normal ones. Furthermore, in the presence of magnetic field, the interplay between superconductivity in such heterostructure and the quantum Hall effect can give rise to intriguing phenomena. These will be the subject of future studies.

We are grateful for help from I. Volotsenko, and useful

discussions with J. Ruhman and N. Trivedi. G.N.D., A.R and A.F were supported by the Israel Science fund, ISF, grant No. 1499/21 and the US-Israel Binational Science Foundation (BSF) grant No. 2020331. U.K., E.W. and E.S. were supported by Israel Science Foundations (ISF) grant No. 993/19, the US-Israel Binational Science Foundation (BSF) grant No. 2016130, and NSF-BSF grant No. 2018726.

-
- [1] J. F. Schooley, W. R. Hosler, and M. L. Cohen, *Phys. Rev. Lett.* **12**, 474 (1964).
- [2] M. Tinkham, *Introduction to superconductivity* (Courier Corporation, 2004).
- [3] Y. Taguchi, A. Kitora, and Y. Iwasa, *Phys. Rev. Lett.* **97**, 107001 (2006).
- [4] Y. Nakagawa, Y. Saito, T. Nojima, K. Inumaru, S. Yamanaka, Y. Kasahara, and Y. Iwasa, *Phys. Rev. B* **98**, 064512 (2018).
- [5] O. Yuli, I. Asulin, O. Millo, D. Orgad, L. Iomin, and G. Koren, *Phys. Rev. Lett.* **101**, 057005 (2008).
- [6] Y. Takada, *Phys. Rev. B* **47**, 5202 (1993).
- [7] M. Calandra, P. Zocante, and F. Mauri, *Phys. Rev. Lett.* **114**, 077001 (2015).
- [8] A. K. Geim and K. S. Novoselov, *Nature Materials* **6**, 183 (2007).
- [9] S. Das Sarma, S. Adam, E. H. Hwang, and E. Rossi, *Rev. Mod. Phys.* **83**, 407 (2011).
- [10] Z. Ovadyahu, *Journal of Physics C: Solid State Physics* **19**, 5187 (1986).
- [11] A. Johansson, G. Sambandamurthy, D. Shahar, N. Jacobson, and R. Tenne, *Physical review letters* **95**, 116805 (2005).
- [12] S. Poran, E. Shimshoni, and A. Frydman, *Phys. Rev. B* **84**, 014529 (2011).
- [13] D. Kowal and Z. Ovadyahu, *Solid state communications* **90**, 783 (1994).
- [14] D. Kowal and Z. Ovadyahu, *Physica C: Superconductivity* **468**, 322 (2008).
- [15] K. Bouadim, Y. L. Loh, M. Randeria, and N. Trivedi, *Nature Physics* **7**, 884 (2011).
- [16] B. Sacépé, T. Dubouchet, C. Chapelier, M. Sanquer, M. Ovidia, D. Shahar, M. Feigel'Man, and L. Ioffe, *Nature Physics* **7**, 239 (2011).
- [17] P. Spathis, H. Aubin, A. Pourret, and K. Behnia, *EPL (Europhysics Letters)* **83**, 57005 (2008).
- [18] D. Sherman, G. Kopnov, D. Shahar, and A. Frydman, *Phys. Rev. Lett.* **108**, 177006 (2012).
- [19] G. Kopnov, O. Cohen, M. Ovidia, K. H. Lee, C. C. Wong, and D. Shahar, *Phys. Rev. Lett.* **109**, 167002 (2012).
- [20] A. Roy, E. Shimshoni, and A. Frydman, *Phys. Rev. Lett.* **121**, 047003 (2018).
- [21] A. Kapitulnik, S. A. Kivelson, and B. Spivak, *Rev. Mod. Phys.* **91**, 011002 (2019).
- [22] G. N. Daptary, E. Walach, E. Shimshoni, and A. Frydman, *arXiv:2009.14603* (2020).
- [23] A. Allain, Z. Han, and V. Bouchiat, *Nature materials* **11**, 590 (2012).
- [24] C. W. J. Beenakker and H. van Houten, *Phys. Rev. Lett.* **66**, 3056 (1991).
- [25] A. Furusaki, *Superlattices and Microstructures* **25**, 809 (1999).
- [26] M. Titov and C. W. J. Beenakker, *Phys. Rev. B* **74**, 041401 (2006).
- [27] A. M. Black-Schaffer and S. Doniach, *Phys. Rev. B* **78**, 024504 (2008).
- [28] F. Mancarella, J. Fransson, and A. Balatsky, *Supercond. Sci. Technol.* **29**, 054004 (2016).
- [29] Y. Takane, *J. Phys. Soc. Jpn.* **89**, 094702 (2020).
- [30] Y. J. Shin, Y. Wang, H. Huang, G. Kalon, A. T. S. Wee, Z. Shen, C. S. Bhatia, and H. Yang, *Langmuir* **26**, 3798 (2010).

**SUPPLEMENTARY INFORMATION -
ENHANCEMENT OF SUPERCONDUCTIVITY
UPON REDUCTION OF CARRIER DENSITY IN
PROXIMITIZED GRAPHENE**

The Supplemental Material presents additional experimental data (section I, II, III) and details regarding the theoretical model (section IV).

I. HALL MEASUREMENT IN SINGLE LAYER GRAPHENE

Polycrystalline single layer graphene were prepared by the CVD technique on copper catalyst and were then transferred to SiO₂/Si substrate. The CVD grown single layer graphene samples were purchased from Graphenea Company which provided Raman data that shows that the entire graphene is single-layer. In Fig. 5 (a), we show the optical image of CVD grown SLG. Figure 5(b) shows the sheet resistance as a function of V_g at $B = 0$ T and $T = 1.7$ K. We identified the Dirac point (DP) as the charge neutrality point (CNP) extracted from the Hall measurement. In Fig. 5(c), Hall resistance R_{xy} is plotted as a function of V_g for different magnetic field and $T = 1.7$ K. Note that the DP is at $V_d = 56$ V. This indicates that graphene is hole doped due to adsorption of atmospheric dopants such as H₂O and O₂ [30]. When the graphene is coated by InO films having increasing electron carrier density, increasing electron doping is induced in the graphene thus shifting the charge neutrality point to negative gate voltages, until, for our superconducting sample Gr/S the CNP reaches -81.5 V (see Fig. 5(d)).

II. RESISTANCE-TEMPERATURE CURVES AT DIFFERENT GATE VOLTAGE FOR SAMPLE GR/S2

Figure 6(a) shows the sheet resistance, normalized by the resistance at 10K, as a function of temperature at different gate voltages relative to the charge neutrality point, CNP, $V_g - V_d$ for sample Gr/S2. The measurements were performed in a wet He-4 system at temperatures down to 1.5 K. For all gate voltages, sample Gr/S2 shows signature of superconductivity at low temperatures. Figure 6(b) shows that T_C (defined as the temperature at which resistance drops to 50% of the normal sheet resistance at 10 K) increases as n decreases and becomes maximum close to the charge neutrality point.

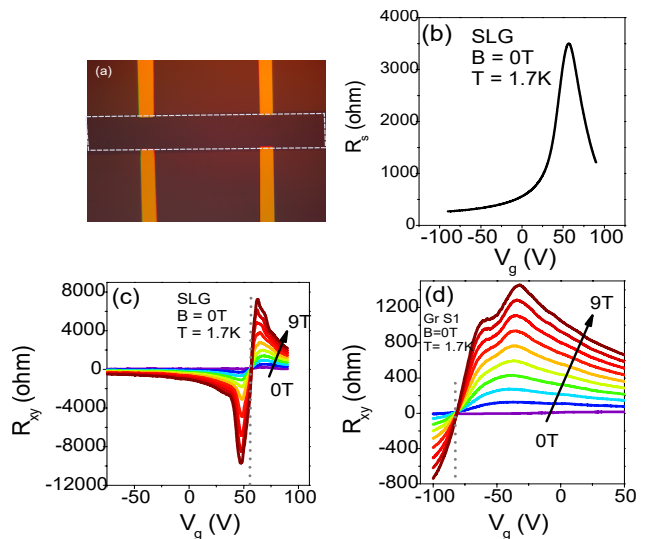


FIG. 5. (a) Optical image of the CVD grown single layer graphene (see dashed white line). (b) Sheet resistance, R_s of SLG as a function of gate voltage, V_g at $B = 0$ T and $T = 1.7$ K. (c) and (d) Hall resistance R_{xy} as a function of V_g of SLG and sample Gr/S at different B (in step of 1T) at $T = 1.7$ K.

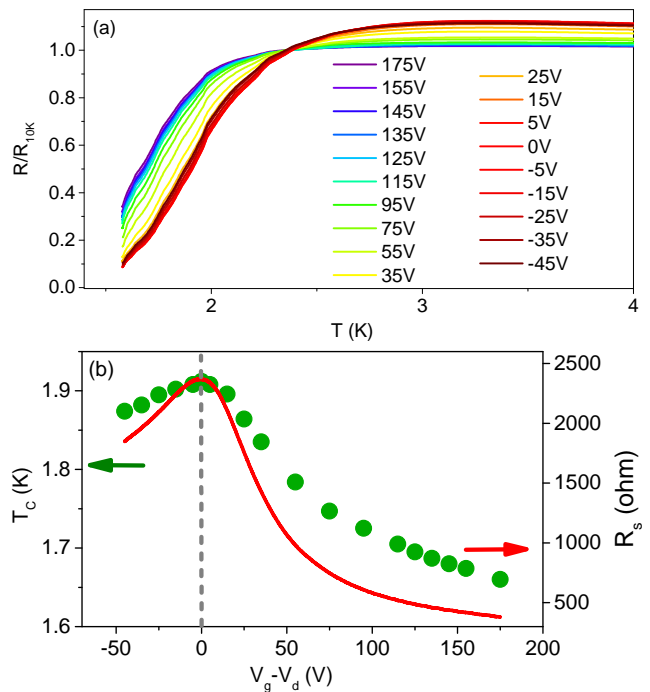


FIG. 6. Sheet resistance, R_s , normalized by the resistance at 10K, as a function of temperature at different gate voltages relative to the CNP, $V_g - V_d$, of sample Gr/S2. (b) T_C and R_s at $T = 5$ K as a function of $V_g - V_d$ measured at $B = 0$ T.

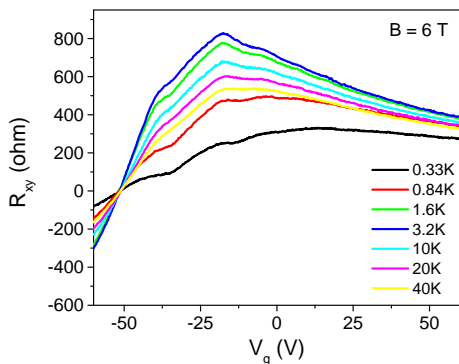


FIG. 7. Hall resistance as a function of gate voltages at different temperatures of sample Gr/S2. The measurements were performed at $B = 6$ T.

III. HALL RESISTANCE - GATE VOLTAGES AT DIFFERENT TEMPERATURE

In Fig. 7, Hall resistance, R_{xy} , is plotted as a function of gate voltages at different temperatures for sample Gr/S2. The measurements were performed at $B = 6$ T. It can be seen that for temperatures below T_c , the Hall effect is suppressed until, for low enough temperatures it is expected to vanish.

IV. THE MODEL FOR A SINGLE JUNCTION

We consider a superconductor-normal-superconductor (SNS) junction of length L (along the x direction) in the ballistic limit [Fig. 8(a)]. Here, the superconducting electrodes correspond to proximitized regions of graphene, with a proximity-induced pairing potential Δ . Our aim is to evaluate the critical current (I_c) in the junction as a function of the gate voltage. We assume that $L \ll \xi$ (the superconducting coherence length). In this limit, the Josephson current is carried mostly by the Andreev bound states (ABS) with energies (ϵ_q^{ABS}) smaller than Δ . Here q could be any generic quantum number labelling the ABS. We consider N-S interfaces parallel to the y direction, and impose periodic boundary conditions along y . We further assume that the width (W) of the junction is much larger than its length L . Under these approximations, $q = 2\pi n/W$ (for $n \in \mathbb{Z}$) denotes the wave vector along y , and there is a single ABS for each q . We stress that we consider these limits only to simplify the calculation of I_c . We do not expect our results to change qualitatively for longer Josephson junctions.

This geometry was also considered by Titov and Beenakker (Ref. [22]). However, unlike previous works, we consider the case where the superconducting and normal regions have opposite polarities. Furthermore, we do not assume that the Fermi energy in the superconducting puddles (E'_F) is much larger than the Fermi energy

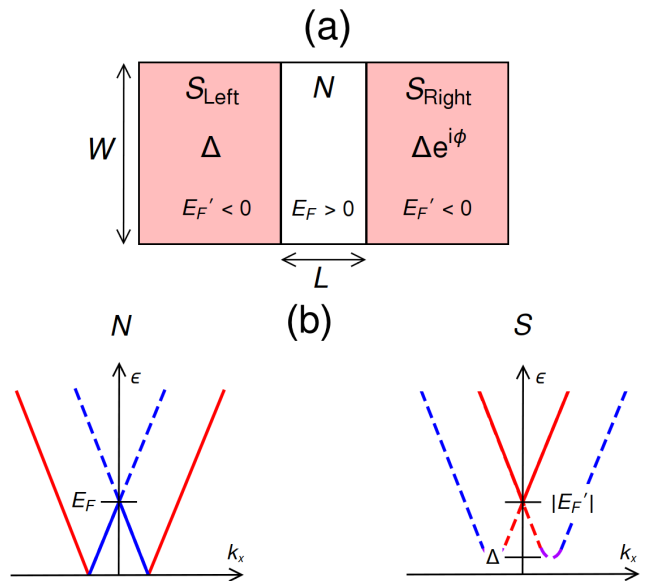


FIG. 8. (a) Schematic of the SNS junction studied here. (b) Low-energy excitations in the normal (N) and superconducting (S) regions (at $q = 0$) of the junction. The solid (dashed) lines denote states corresponding to conduction (valence) bands, while the red (blue) color denote the electron-like (hole-like) states in the Nambu representation. Note that the N (S) region is considered to be electron-doped (hole-doped), so that $E_F > 0$ ($E'_F = E_F - U < 0$). Therefore the excitations with largest k_x , are electron-like states of the conduction band (hole-like states of the valence band) in N (S) regions.

of the normal regions (E_F). Our analysis relies on completely general solutions of the BdG equations in the superconducting regions. By contrast, the wave functions employed in Ref. [22] were limiting cases of Eqs. (6-7) below.

For a fixed phase difference (ϕ) between the superconductors, the junction supports an equilibrium supercurrent, $I(\phi)$, which depends on the ABS spectrum through,

$$I(\phi) = -4 \frac{e}{\hbar} \sum_q \frac{\partial \epsilon_q^{\text{ABS}}}{\partial \phi}. \quad (2)$$

The factor of 4 accounts for the spin and valley degeneracies. The critical current, I_c , is the largest value of $I(\phi)$. Therefore our main task is to evaluate the energy of subgap ABS as a function of q and ϕ .

Due to Andreev reflection at the N-S interfaces, a general state inside the normal region of graphene is a superposition of electrons and holes from different valleys. For brevity, we only consider states involving electrons from a given valley and with a fixed spin polarization. The spin-valley degeneracy is incorporated in the end through the factor of 4 in Eq. (2). Thus the dynamics of the normal

region may be described through the Hamiltonian,

$$H_N = \begin{pmatrix} H_0 - E_F & 0 \\ 0 & E_F - H_0 \end{pmatrix}, \quad (3)$$

where $H_0 = -i(\sigma_x \partial_x + \sigma_y \partial_y)$, and σ represents the sublattice degree of freedom. Throughout our analysis $\hbar v_F$ is set to 1, and we employ the Nambu representation. The upper (lower) block of H_N corresponds to electrons (holes). The Hamiltonian for electrons in the other valley is similar to H_N with $H_0 \rightarrow -i(\sigma_x \partial_x - \sigma_y \partial_y)$. Eq. (3) has 4 eigenvectors for a given energy (ϵ) and transverse wave vector (q), corresponding to the left and right moving electrons ($\psi_{e,L}$ and $\psi_{e,R}$) and holes ($\psi_{h,L}$ and $\psi_{h,R}$). Consequently a general state in the normal region with a given ϵ and q is,

$$\Psi_N(\epsilon, q) = a_+ \psi_{e,R} + a_- \psi_{e,L} + b_+ \psi_{h,R} + b_- \psi_{h,L}. \quad (4)$$

Note that the dependence on position has been suppressed for brevity.

The proximitized regions of graphene are described by the Hamiltonian,

$$H_S = \begin{pmatrix} H_0 - E'_F & \Delta e^{i\phi} \\ \Delta e^{-i\phi} & E'_F - H_0 \end{pmatrix} \quad (5)$$

where, E'_F is the Fermi energy in the superconducting region. E'_F is positive (negative) in electron-doped (hole-doped) superconductors. For an interface between a metallic superconductor (such as a grain of Sn) and graphene, E'_F is not only positive but $E'_F \gg E_F$. This is the limit considered in Ref. [22]. In our case, $E'_F = E_F - U$ is assumed to be negative. We assume that the electrostatic shift (U) is fixed by the coupling between graphene and InO, while E_F (and consequently E'_F) may be tuned using external gates.

H_S has four eigenvectors for a given ϵ and q . For $\epsilon < \Delta$ the wave vector along x : p_x , is complex. Hence, inside a given superconductor only the two solutions which decay with distance away from the interface are physically relevant for our setup. We label the physical solutions as $\psi_{\pm, L/R}$, where the sign \pm labels the two solutions in the superconductor to the left (L) or right (R) of the normal region. Solving the eigenvalue equation corresponding to H_S , we find,

$$\psi_{+, L/R} = e^{i(k_x x + qy) - \zeta \kappa x} \begin{pmatrix} e^{i\zeta \times \text{sign}(E'_F)\beta} \\ d_+ e^{i\zeta \times \text{sign}(E'_F)\beta} \\ e^{-i\phi} \\ d_+ e^{-i\phi} \end{pmatrix}, \quad (6)$$

$$\psi_{-, L/R} = e^{i(-k_x x + qy) - \zeta \kappa x} \begin{pmatrix} e^{-i\zeta \times \text{sign}(E'_F)\beta} \\ d_- e^{-i\zeta \times \text{sign}(E'_F)\beta} \\ e^{-i\phi} \\ d_- e^{-i\phi} \end{pmatrix}. \quad (7)$$

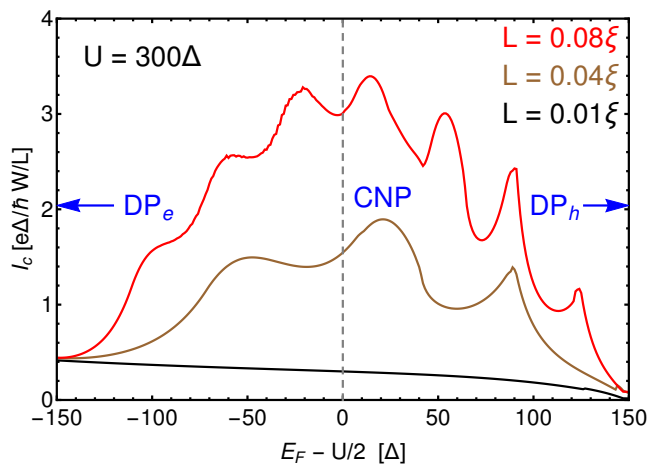


FIG. 9. The critical current (I_c) as a function of the Fermi energy relative to the CNP (in units of Δ). The different curves denote I_c for junctions of different lengths. The leftmost (rightmost) energy corresponds to the DP_e (DP_h). At the CNP, the carrier densities in the electron and hole regions are equal, so that the average density is zero. Note that for sufficiently large L , I_c has an overall maxima close to the CNP, along with several length-dependent oscillations which arise from the Andreev bound states. These length-dependent features would only be observable in very clean devices comprising a single Josephson junction. In the disordered samples considered here, we only observe the envelope function of I_c which is maximal close to the CNP.

Here we have used $\zeta = +1(-1)$ for the superconductor on the right (left), $\beta = \arccos[\epsilon/\Delta]$, $k_x = |\text{Re}[p_x]|$, and $\kappa = |\text{Im}[p_x]|$. Finally,

$$d_{\pm} = \frac{E'_F \pm i\zeta \times \text{sign}(E'_F) \sqrt{\Delta^2 - \epsilon^2}}{p_{x\pm} - iq}. \quad (8)$$

Thus, the most general wave function (given ϵ and q) in the two superconducting regions is,

$$\Psi_{S,L/R}(\epsilon, q) = c_{+,L/R} \psi_{+,L/R} + c_{-,L/R} \psi_{-,L/R}. \quad (9)$$

As an aside we note that, in the limit $E'_F \gg E_F$, $\Delta > 0$,

$$d_{\pm} \approx \pm e^{\pm i\gamma} \quad \text{where } \gamma = \sin^{-1} \left(\frac{q}{|E'_F|} \right). \quad (10)$$

In this limit, the solutions above [Eqs. (6-7)] reduce to those given in Ref. [22].

To solve for the ABS we impose continuity conditions on the wave functions, Ψ_S and Ψ_N , at the two N-S interfaces. For a given q , the boundary conditions $\Psi_{SL}(x = -L/2) = \Psi_N(x = -L/2)$ and $\Psi_{SR}(x = L/2) = \Psi_N(x = L/2)$ can be satisfied simultaneously only for some discrete values of $\epsilon < \Delta$. These are the ABS localized in the normal region. We find the ABS spectrum ϵ_q^{ABS} by numerically solving the equations for the coefficients ($a_{\pm}, b_{\pm}, c_{\pm, L/R}$) which arise from the boundary conditions. The current is then found by replacing the

derivative $\partial\epsilon/\partial\phi$ [in Eq. (2)] with a (central) finite difference expression.

Fig. 9 shows the variation of I_c with $E_F - U/2$ for different values of L . Note that in our notation, $E_F - U/2 = -U/2$ corresponds to DP_e (the Dirac point in normal regions of graphene, defined by $E_F = 0$), while $E_F - U/2 = U/2$ corresponds to DP_h (the Dirac point in superconducting regions of graphene, defined by $E'_F = 0$). In between these values, $E_F > 0$ while $E'_F < 0$. Our results clearly show that while several details of the I_c vs. E_F curve depend on the length L of the junction, the critical current (for $\frac{U}{\hbar v_F} L \gg 1$) is maximal close to

the average CNP, defined as $E_F = U/2 = E'_F$. Such L -dependent features would be suppressed in an array of several junctions with a random variation of lengths. Therefore Fig. 4 of the main text depicts I_c averaged over several values of L (keeping $\bar{L} \ll \xi$). We stress that the average I_c should be maximal close to the CNP, but since there is no symmetry relating the DP_e and DP_h , there is no reason to expect that maximal value to be exactly at the CNP. Furthermore although the averaging procedure strongly suppresses the oscillations, some small wiggles would be left behind (which are manifest in Fig. 4 of the main text).